Received January 1997
Revised May 1997

Numerical study of laminar natural convection in tilted enclosure with transverse magnetic field

N.M. Al-Najem, K.M. Khanafer, and M.M. El-Refaee
Kuwait University College of Engineering and Petroleum, Department of Mechanical and Industrial Engineering, Safat, Kuwait

Nomenclature

$a_{i,j}$ = coefficient of finite difference equation at point (i, j) in a grid
A = function of power law
$\underline{b}$ = right hand side of finite difference equation
B = magnetic induction, tesla
B_o = constant magnetic field
c_p = specific heat, J/(kg. K)
g = gravitational acceleration, m/s^2
Gr = grashof number, $\frac{g\beta \Delta T H^2}{\nu^2}$
$\bar{h}$ = average heat transfer coefficient
H = enclosure length, m
Ha = Hartmann number, $Ha = B_o H \sqrt{\frac{\sigma}{\rho_o \nu}}$
$\vec{J}$ = current density, A/m^2
K = thermal conductivity of fluid, W/(m. K)
L = characteristic length, m
M = grids number in x-direction
N = grids number in y-direction
$\overline{Nu}$ = average Nusselt number,

$$\overline{Nu} = \frac{\bar{h}\,H}{K} = -\int_0^1 \frac{\partial \theta}{\partial X}\, dY$$

P = pressure, Pa.
Pr = Prandtl number, $\frac{\nu}{\alpha}$
Re_m = magnetic Reynold number, $\frac{UL}{\nu_e}$
T = temperature, °C
T_o = reference temperature, °C
ΔT = temperature difference, $(T_H - T_C)$
t = time, s
u = velocity in x-direction
$\underline{v}$ = velocity in y-direction
$\vec{V}$ = velocity vector
U = dimensionless velocity $\frac{u}{\sqrt{g\beta \Delta T H}}$
V = dimensionless velocity $\frac{v}{\sqrt{g\beta \Delta T H}}$
U_c = dimensionless velocity in x-direction at mid-width of enclosure
V_c = dimensionless velocity in y-direction at mid-width of enclosure
x, y = Cartesian coordinates
X, Y = dimensionless Cartesian coordinates, $\frac{(x, y)}{H}$

Greek symbols

α = enclosure angle inclination
α_f = thermal diffusivity, m^2/s
β = coefficient of thermal expansion of fluid, K^{-1}
μ = dynamic viscosity, Pa. s
μ_e = magnetic permeability
ν = kinematic viscosity, $\frac{\mu}{\rho}$
θ = dimensionless temperature, $\frac{T - T_C}{T_H - T_C}$
ψ = stream function, m^2/s
Ψ = dimensionless stream function, $\frac{\psi}{H\sqrt{g\beta \Delta T H}}$
ω = dimensionless vorticity, $\frac{\Omega H}{\sqrt{g\beta \Delta T H}}$
τ = dimensionless time, $\frac{t\sqrt{g\beta \Delta T H}}{H}$
ρ_o = density at reference temperature To
σ = electrical conductivity, mho

Subscripts

C = cold wall
H = hot wall
o = value at reference temperature
i = X location of a grid point
j = Y location of a grid point

International Journal of Numerical
Methods for Heat & Fluid Flow
Vol. 8 No. 6, 1998, pp. 651–672.

Introduction

Natural convection heat transfer in enclosures has received considerable attention in the past few decades, Ostrach[1] and Catton[2]. The interest in such problems comes from their importance in numerous technical and engineering applications, such as cooling of electrical equipment, electronic packaging, nuclear reactors, solar collectors and crystals manufacturing[3-12]. In material manufacturing technology researchers apply external magnetic field to suppress unavoidable convection currents which leads to better control of crystal quality.

Ozoe and Maruo[13] investigated numerically the natural convection of an electrically conducting fluid in the presence of magnetic field at low Prandtl number. The Nusselt numbers obtained are correlated in terms of Rayleigh, Prandtl and Hartmann numbers. Three dimensionality and effect of magnetic direction are examined by Ozoe and Okada[14]. It is found that optimal suppression of the convection currents occurs when the external magnetic field is parallel to the direction of the heat flow. Vasseur *et al.*[15] studied analytically as well as numerically the effect of transverse magnetic field on buoyancy-driven convection in an inclined two-dimensional tall cavity (i.e. aspect ratio AR = 4). They achieved good agreement with the one dimensional parallel flow solution developed by Cormack *et al.*[16].

Alchaar *et al.*[17] investigated the effect of the magnetic drag on the convection currents in vertical differentially heated shallow cavity. A standard finite difference scheme is used to predict the solutions for a wide range of Rayleigh number Ra (10^2-10^5), Hartmann number Ha ($0 < Ha < 100$) and Prandtl number ($0.005 < Pr < 1$). The results compared well with a closed form solution obtained by Garandet *et al.*[18]. Rudraiah *et al.*[19] used modified alternating direction implicit (ADI) finite difference scheme to solve the vorticity-stream function formulation of natural convection inside a rectangular enclosure in the presence of a magnetic field. The two vertical side walls are held isothermally at temperatures T_H and T_C, while the top and bottom walls are adiabatic. Numerical predictions are obtained for a wide range of Grashof number and Hartmann number with Prandtl number Pr = 0.733. Dominant convection with vertical thermal stratification in the core region is also predicted for high Grashof number and low Hartmann number. The numerical results showed that of the magnetic field suppresses the rate of convective heat transfer. The mechanism of the crystal growth in the presence of magnetic field is examined in early 1980 by Oreper and Szekely[20] . They have found that the magnetic field can suppress natural convection and that the strength of the magnetic field is one of the important factors during the crystal formation. Alchaar *et al.*[21] studied numerically two dimensional natural convection in a shallow cavity heated from below in the presence of inclined magnetic field at AR = 6 for $1.8 \times 10^3 < Ra < 3 \times 10^4$, $0 < Ha < 35$, and $0.005 < Pr < 1$. The numerical results showed that the effect of the magnetic field is to reduce the heat transfer and inhibit the onset of the convection current. Further, the convection modes inside the cavity are found to depend strongly upon both the strength and orientation of the magnetic field. Using horizontal magnetic field is found to be the most effective in suppressing the convective flow.

Recently, Garandet *et al.*[18] studied the influence of transverse magnetic field on buoyancy-driven convection in a shallow two dimensional cavity heated isothermally from the sides. The velocity and temperature profiles in the core of the enclosure are predicted analytically based on the one dimensional parallel flow approximation. The circulating part of the flow near the vertical walls of the enclosure is examined by means of a series expansion. A summary of previously published related work on the subject of the problem under investigation can be found in Table I.

The main objective of the present work is to examine the influence of the magnetic field on the heat transfer process inside tilted enclosures for a wide range of inclination angles at moderate and high Grashof numbers. Therefore, a two-dimensional numerical model is developed to solve the vorticity, stream function and temperature governing equations of buoyancy-driven natural convection flow inside a cavity.

Problem formulation

Consider two-dimensional square enclosure with sides of length H filled with an electrically conducting fluid as shown in Figure 1. The horizontal walls of the cavity are assumed to be perfectly insulated, while the vertical walls are kept isothermal with the left wall at high temperature T_H and the right wall at low temperature T_C. The fluid is permeated by a uniform external magnetic field Bo. The resulting convective flow is governed by the combined mechanism of the driving buoyancy force and the electromagnetic retarding force. The magnetic Reynolds number is assumed to be small so that the induced magnetic field produced by the motion of the electrically conducting fluid is negligible compared to the applied magnetic field Bo. The flow is assumed to be laminar, unsteady, incompressible, with constant physical properties. The density variation only in the body force term according to the Boussinesq

Reference	Geometry AR	2D or 3D	α	Ha	Gr or Ra	Pr
Ozoe and Marue[13]	1	2	0°	$1 \leq Ha \leq 10^3$	$10^4 \leq Ra \leq 10^6$	0.054
Ozoe and Okada[14]	1	3	0°	$0 \leq Ha \leq 500$	$Ra = 10^6, 10^7$	0.054
Vasseur *et al.*[15]	4	2	$0° \leq \alpha \leq 180°$	$1 \leq Ha \leq 500$	$1 \leq R^* \leq 500$	0.72
Alchaar *et al.*[17]	$1 \leq AR \leq 6$	2	0°	$1 \leq Ha \leq 100$	$10^2 \leq Ra \leq 10^5$	$0.005 \leq Pr \leq 1$
Rudraiah *et al.*[19]	1	2	0°	$0 \leq Ha \leq 100$	$2 \times 10^4 \leq Gr \leq 2 \times 10^6$	0.733
Oreper and Szekely[20]	1	2	0°	$0 \leq N^+ \leq 100$	$Gr = 8.2 \times 10^6$	0.014
Alchaar *et al.*[21]	6	2	0°	$0 \leq Ha \leq 35$	$1.8| 10^3 \leq Ra \leq 3 \times 10^4$	$0.005 \leq Pr \leq 1$

Note:
$R^* = Ra/Ha^2$, $N^+ = Ha^2/\sqrt{Gr}$, AR: aspect ratio

Table I.
Review of previous work on the effect of the magnetic field on free convection inside enclosures

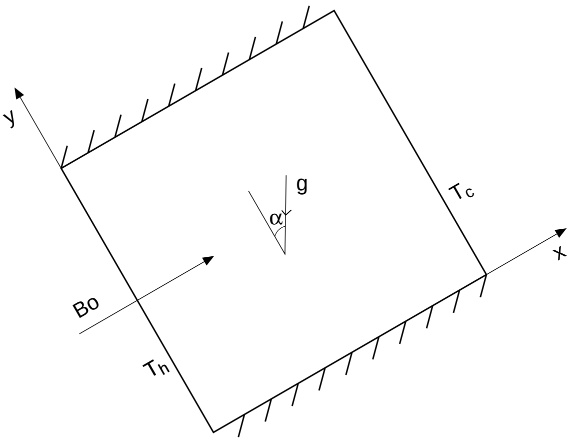

Figure 1.
Geometry and coordinates of tilted cavity configuration with magnetic effect

approximation. Further, pressure work, Joule heating and viscous dissipation are to be assumed negligible[22].

The pertinent governing equations in this study are based on the conservation laws of mass, linear momentum, energy and magnetic induction are given in dimensionless form as

$$\omega = -\left(\frac{\partial^2}{\partial X^2} + \frac{\partial^2}{\partial Y^2}\right)\Psi \tag{1}$$

$$U = \frac{\partial \Psi}{\partial Y}, \quad V = -\frac{\partial \Psi}{\partial X} \tag{2}$$

$$\frac{\partial \omega}{\partial \tau} + U\frac{\partial \omega}{\partial X} + V\frac{\partial \omega}{\partial Y} = \frac{1}{\sqrt{Gr}}\left(\frac{\partial^2 \omega}{\partial X^2} + \frac{\partial^2 \omega}{\partial Y^2}\right) + \left(\frac{\partial \theta}{\partial X}\cos\alpha - \frac{\partial \theta}{\partial Y}\sin\alpha\right) - \frac{Ha^2}{\sqrt{Gr}}\frac{\partial V}{\partial X} \tag{3}$$

$$\frac{\partial \theta}{\partial \tau} + U\frac{\partial \theta}{\partial X} + V\frac{\partial \theta}{\partial Y} = \frac{1}{Pr\sqrt{Gr}}\left(\frac{\partial^2 \theta}{\partial X^2} + \frac{\partial^2 \theta}{\partial Y^2}\right) \tag{4}$$

The effect of the electromagnetic field is introduced into the equations of motion through $\vec{J} \times \vec{B}$ the term, which is the vector product of the electric current density and magnetic field inductance $\vec{B}$ and represents the Lorentz force. The electric current density $\vec{J}$ is calculated from Ohm's phenomenological law as[23]:

$$\vec{J} = \sigma(\vec{E} + \vec{V} \times \vec{B}) \tag{5}$$

In the present investigation the magnetic Reynolds number is very small (i.e. $Re_m << 1$) in most of the engineering applications and defined as:

$$Re_m = \frac{VL}{\nu_e}$$

where

$$\nu_e = \frac{1}{\sigma\mu_e}.$$

As discussed by Garandet *et al.*[18], the harmonic equation for the electric potential, $\nabla\varphi = 0$, is valid in the melt as well as in the neighboring solid media. The unique solution of the harmonic equation is $\vec{\nabla}\phi = 0$ since there is always an electrically insulating boundary on which $\frac{\partial\varphi}{\partial n} = 0$ around the enclosure. It follows that the electric field vanishes everywhere.

The general transport equations of the vorticity or energy can be written in a canonical form as[24]:

$$\frac{\partial\phi}{\partial\tau} + \frac{\partial}{\partial X}[U\phi - \Gamma_\phi \frac{\partial\phi}{\partial X}] + \frac{\partial}{\partial Y}[V\phi - \Gamma_\phi \frac{\partial\phi}{\partial Y}] = S_\phi \tag{6}$$

where ϕ stands for ω or θ and Γ_ϕ and S_ϕ are

$$\Gamma_\theta = \frac{1}{Pr\sqrt{Gr}} \qquad S_\theta = 0$$

$$\Gamma_\omega = \frac{1}{\sqrt{Gr}} \qquad S_\omega = -\frac{Ha^2}{\sqrt{Gr}}\frac{\partial V}{\partial X} + (\frac{\partial\theta}{\partial X}\cos\alpha - \frac{\partial\theta}{\partial Y}\sin\alpha)$$

The boundary conditions are

$$U = V = \Psi = 0$$

on all boundaries

$$\begin{array}{llll} \frac{\partial\theta}{\partial Y} = 0 & @ & Y = 0, 1 & \text{for all } X \\ \theta = 1 & @ & X = 0 & \text{for all } Y \\ \theta = 0 & @ & X = 1 & \text{for all } Y \end{array} \tag{7}$$

Numerical algorithms

In the present work, the control volume algorithm[25] is used to solve the two-dimensional transient governing equations (1-4) subjected to the boundary conditions given in equation (7). In this algorithm, alternating direct implicit procedure (ADI) along with the successive grid refinement scheme are respectively implemented in the spatial and temporal environment to accelerate the solution convergence towards steady state. Additionally, the application of the ADI procedure enhances the accuracy of the solution since it allows the power law to be applied locally in a one-dimensional sense for each sweep in the coordinate directions. The resulting finite difference of equation (6) in the X and Y directions are given as:

$$\left.\begin{aligned}
-a_{i-1,j}^{n+\frac{1}{2}}\phi_{i-1,j}^{n+\frac{1}{2}}+a_{i,j}^{n+\frac{1}{2}}\phi_{i,j}^{n+\frac{1}{2}}-a_{i+1,j}^{n+\frac{1}{2}}\phi_{i+1,j}^{n+\frac{1}{2}}&=b^{n}\\
-a_{i,j-1}^{n+1}\phi_{i,j-1}^{n+1}+a_{i,j}^{n+1}\phi_{i,j}^{n+1}-a_{i,j+1}^{n+1}\phi_{i,j+1}^{n+1}&=b^{n+\frac{1}{2}}
\end{aligned}\right\}\tag{8}$$

where the subscripts i and j denote the X and Y locations of the grid point, respectively. The superscripts n, n + $\frac{1}{2}$, n + 1 denote respectively old time, advanced half-time step and advanced full-time step. The coefficients of equation (8) are expressed as[26]

$$\left.\begin{aligned}
a_{i-1,j}^{n+\frac{1}{2}}&=\frac{\Delta\tau\,\Gamma_{\phi}}{\Delta X^{2}}A\left(\left|P_{i-\frac{1}{2},j}^{n+\frac{1}{2}}\right|\right)+\frac{\Delta\tau}{\Delta X}\left[\left[U_{i-\frac{1}{2},j}^{n+\frac{1}{2}},o\right]\right]\\
a_{i+1,j}^{n+\frac{1}{2}}&=\frac{\Delta\tau\,\Gamma_{\phi}}{\Delta X^{2}}A\left(\left|P_{i+\frac{1}{2},j}^{n+\frac{1}{2}}\right|\right)+\frac{\Delta\tau}{\Delta X}\left[\left[-U_{i+\frac{1}{2},j}^{n+\frac{1}{2}},0\right]\right]\\
a_{i,j}^{n+\frac{1}{2}}&=2+a_{i-1,j}^{n+\frac{1}{2}}+a_{i+1,j}^{n+\frac{1}{2}}\\
b^{n}&=2\phi_{i,j}^{n}+\frac{\Delta\tau\,\Gamma_{\phi}}{\Delta Y^{2}}\left\{A\left(\left|P_{i,j+\frac{1}{2}}^{n}\right|\right)\cdot\left(\phi_{i,j+1}^{n}-\phi_{i,j}^{n}\right)+A\left(\left|P_{i,j-\frac{1}{2}}^{n}\right|\right)\left(\phi_{i,j-1}^{n}-\phi_{i,j}^{n}\right)\right\}\\
&+\frac{\Delta\tau}{\Delta Y}\left\{\left[\left[-V_{i,j+\frac{1}{2}}^{n},0\right]\right]\left(\phi_{i,j+1}^{n}-\phi_{i,j}^{n}\right)+\left[\left[V_{i,j-\frac{1}{2}}^{n},0\right]\right]\left(\phi_{i,j-1}^{n}-\phi_{i,j}^{n}\right)\right\}+\Delta\tau.S_{\phi}^{n}
\end{aligned}\right\}\tag{9a}$$

$$\left.\begin{aligned}
a_{i,j-1}^{n+1}&=\frac{\Delta\tau\,\Gamma_{\phi}}{\Delta Y^{2}}A\left(\left|P_{i,j-\frac{1}{2}}^{n+1}\right|\right)+\frac{\Delta\tau}{\Delta Y}\left[\left[V_{i,j-\frac{1}{2}}^{n+1},0\right]\right]\\
a_{i,j+1}^{n+1}&=\frac{\Delta\tau\,\Gamma_{\phi}}{\Delta Y^{2}}A\left(\left|P_{i,j+\frac{1}{2}}^{n+1}\right|\right)+\frac{\Delta\tau}{\Delta Y}\left[\left[-V_{i,j+\frac{1}{2}}^{n+1},0\right]\right]\\
a_{i,j}^{n+1}&=2+a_{i,j-1}^{n+1}+a_{i,j+1}^{n+1}\\
b^{n+\frac{1}{2}}&=2\phi_{i,j}^{n+\frac{1}{2}}+\frac{\Delta\tau\,\Gamma_{\phi}}{\Delta X^{2}}\left\{A\left(\left|P_{i+\frac{1}{2},j}^{n+\frac{1}{2}}\right|\right)\left(\phi_{i+1,j}^{n+\frac{1}{2}}-\phi_{i,j}^{n+\frac{1}{2}}\right)+A\left(\left|P_{i-\frac{1}{2},j}^{n+\frac{1}{2}}\right|\right)\cdot\left(\phi_{i-1,j}^{n+\frac{1}{2}}-\phi_{i,j}^{n+\frac{1}{2}}\right)\right\}\\
&+\frac{\Delta\tau}{\Delta X}\left\{\left[\left[-U_{i+\frac{1}{2},j}^{n+\frac{1}{2}},0\right]\right]\left(\phi_{i+1,j}^{n+\frac{1}{2}}-\phi_{i,j}^{n+\frac{1}{2}}\right)+\left[\left[U_{i-\frac{1}{2},j}^{n+\frac{1}{2}},0\right]\right]\left(\phi_{i-1,j}^{n+\frac{1}{2}}-\phi_{i,j}^{n+\frac{1}{2}}\right)\right\}+\Delta\tau.S_{\phi}^{n+\frac{1}{2}}
\end{aligned}\right\}\tag{9b}$$

where

$$\left.\begin{aligned} U_{i\pm\frac{1}{2},j} &= \frac{1}{2}(U_{i,j} + U_{i\pm1,j}) \\ V_{i,j\pm\frac{1}{2}} &= \frac{1}{2}(V_{i,j} + V_{i,j\pm1}) \\ U_{i,j}^{n+\frac{1}{2}} &= \frac{1}{2}(U_{i,j}^{n} + U_{i,j}^{n+1}) \end{aligned}\right\} \tag{10a}$$

and

$$\left.\begin{aligned} p_{i\pm\frac{1}{2},j} &= \frac{\Delta X}{\Gamma_\phi}\frac{1}{2}(U_{i,j} + U_{i\pm1,j}) \\ p_{i,j\pm\frac{1}{2}} &= \frac{\Delta Y}{\Gamma_\phi}\frac{1}{2}(V_{i,j} + V_{i,j\pm1}) \end{aligned}\right\} \tag{10b}$$

The function $A(|P|)$ in equations (9a, 9b) is given by the following expression[27]:

$$A(|P|) = [[\,0, (1 - 0.1|P|)^5\,]] \tag{11}$$

where the operator [[a, b]] denotes the greater of a and b. To complete the discretization process, the flow kinematics equation (1) is discretized using central finite difference. The final form of the equations becomes

$$\Psi_{i,j}^{n+1} = (\Psi_{i,j}^{n+1})^k + \frac{\lambda}{2(1+\varepsilon^2)} \left[\begin{aligned} &(\Psi_{i+1,j}^{n+1})^k + (\Psi_{i-1,j}^{n+1})^{k+1} + \varepsilon^2\{(\Psi_{i,j+1}^{n+1})^k + (\Psi_{i,j-1}^{n+1})^{k+1}\} \\ &\quad - 2(1+\varepsilon^2)(\Psi_{i,j}^{n+1})^k + \Delta X^2\,\omega_{i,j}^{n+1} \end{aligned}\right] \tag{12}$$

where ε is the ratio of the step sizes, so that $\varepsilon = \Delta X/\Delta Y$, n and k are the time step and the iteration step, and λ represents the relaxation factor which is given as

$$\lambda = \frac{8 - 4\sqrt{4 - \delta^2}}{\delta^2} \tag{13}$$

where

$$\delta = \cos\left(\frac{\pi}{M}\right) + \cos\left(\frac{\pi}{N}\right) \tag{14}$$

where M and N are the total number of grid points along the X and Y-directions respectively. Once $\Psi_{i,j}^{n+1}$ is calculated, $U_{i,j}^{n+1}$, $V_{i,j}^{n+1}$ are computed as

$$\left.\begin{aligned} U_{i,j}^{n+1} &= \frac{\Psi_{i,j+1}^{n+1} - \Psi_{i,j-1}^{n+1}}{2\Delta Y} \\ V_{i,j}^{n+1} &= \frac{\Psi_{i-1,j}^{n+1} - \Psi_{i+1,j}^{n+1}}{2\Delta X} \end{aligned}\right\} \tag{15}$$

The vorticity on the boundaries is computed according to the following expressions obtained from equations (1) and (2)

$$\left.\begin{aligned} \omega_{i,1} &= \frac{(-4\,U_{i,2} + U_{i,3})}{2\Delta Y} \\ \omega_{i,N} &= \frac{(4U_{i,N-1} - U_{i,N-2})}{2\Delta Y} \\ \omega_{1,j} &= \frac{(4V_{2,j} - V_{3,j})}{2\Delta X} \\ \omega_{M,j} &= \frac{(-4V_{M-1,j} - V_{M-2,j})}{2\Delta X} \end{aligned}\right\} \tag{16}$$

Solution procedure

(1) Use the temperatures of the previous time step as an initial guess. For the first time step, the initial temperature will be used to initiate the computation.

(2) Choose the trial values for U^n, V^n for the first approximation of U^{n+1}, V^{n+1}.

(3) Compute the new values of the temperature at each grid point using equation (8) with ϕ to stand for θ.

(4) Use the values of the vorticities of the previous time step as an initial guess. For the first time step, the vorticities are assumed to be zero everywhere to initiate the solution.

(5) Use the values of U^{n+1}, V^{n+1} and θ^{n+1} to compute the values of ω^{n+1} from equation (8) at the interior grid points.

(6) Solve the stream function equation (12) using the new values of the vorticities obtained in step (5) above.

(7) Determine the new values of U^{n+1}, V^{n+1} and from the values of ψ^{n+1} using central difference scheme given by equations (15).

(8) Compute the new boundary vorticities using the new values of U^{n+1} and V^{n+1} obtained in step (7) above using equation (16).

(9) Use the new values of U^{n+1} and V^{n+1} to repeat steps 5 to 8. Check convergence of ω^{n+1} and θ^{n+1}, if not converged repeat steps 5 to 8.

(10) Repeat steps 4 to 9 for advancing time levels until steady state convergence is achieved.

Results and discussion

The present algorithm is validated against the finite volume solution of Barakos *et al.*[11] and the finite element solution of the Flotran package in the absence of the magnetic field (Ha = 0) for Rayleigh number 1×10^4 and Pr = 0.71 as shown in Figure 2. Moreover, the algorithm is verified with Rudraiah *et al.*'s[19] work for a rectangular enclosure in the presence of magnetic field and the comparison is given in Figures 3 and 4. It is evident from these figures that the present results are in good agreement with the standard benchmark solution. Table II clearly demonstrates a good agreement of the average Nusselt number between the present work and the available numerical results. Numerical experiments showed that an equally spaced grid mesh of 41×41 is adequate to describe correctly the flow and heat transfer processes. Further increase in the number of grids, produce essentially the same results as discussed earlier by El-Refaee *et al.*[25]. The convergence criterion to reach steady-state solution is the standard relative error based on the maximum-norm given by

$$\lambda = \frac{\left\|\Omega^{n+1} - \Omega^{n}\right\|_{\infty}}{\left\|\Omega^{n+1}\right\|_{\infty}} + \frac{\left\|\theta^{n+1} - \theta^{n}\right\|_{\infty}}{\left\|\theta^{n+1}\right\|_{\infty}} \leq 10^{-6} \quad (17)$$

where the operator $\|\eta\|_{\infty}$ indicates the maximum absolute value of the variable over all the grid points in the computational domain.

In this section, some representative results are presented to illustrate the effects of various controlling parameters on the heat transfer and fluid flow processes inside the enclosure. These controlling parameters include inclination angle, Hartmann number, and Grashof number. The reader should consult reference[28] for more details on numerical results.

The influence of the transverse magnetic field (Ha) on the flow patterns and isotherms inside the cavity at moderate Grashof number (Gr = 1×10^4) is shown in Figures 5 and 6. It is evident from these figures that the intensity of the core convection is considerably decreased due to the drag force induced by the magnetic field; as indicated by a weak distortion of the isothermal lines. This effect is more pronounced at smaller inclination angles ($0 < |\alpha| < 30°$) and diminishes considerably for higher inclination angle ($|\alpha| > 60°$) as depicted in Figures 5 and 6. For vertical cavities ($\alpha = 0°$) the core vortex is elongated vertically with the increase of Hartman number. This process continues until this vortex finally breaks up in two secondary vortices, see Figure 7. Further, the isotherms at Ha = 50 are almost parallel to the vertical walls, indicating that most of the heat transfer process is carried out by conduction. From the above,

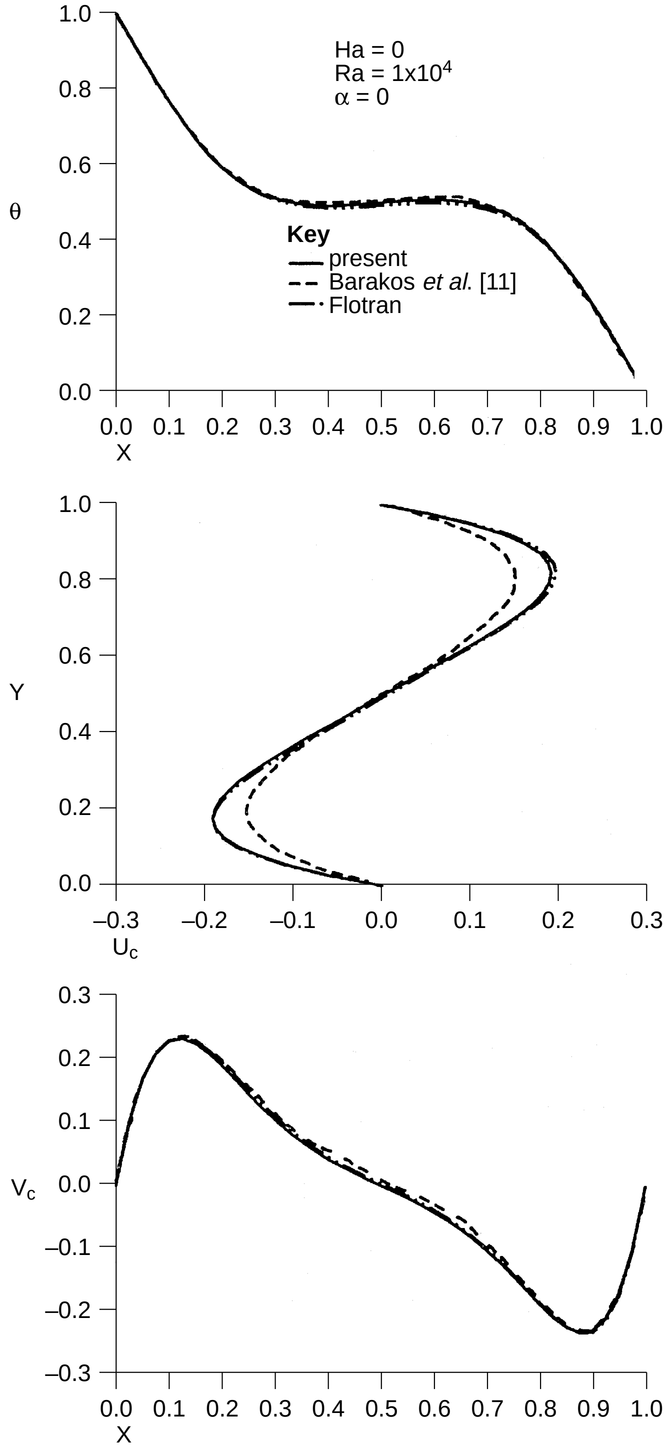

Figure 2.
Comparison of the present temperature and velocity profiles with other solutions

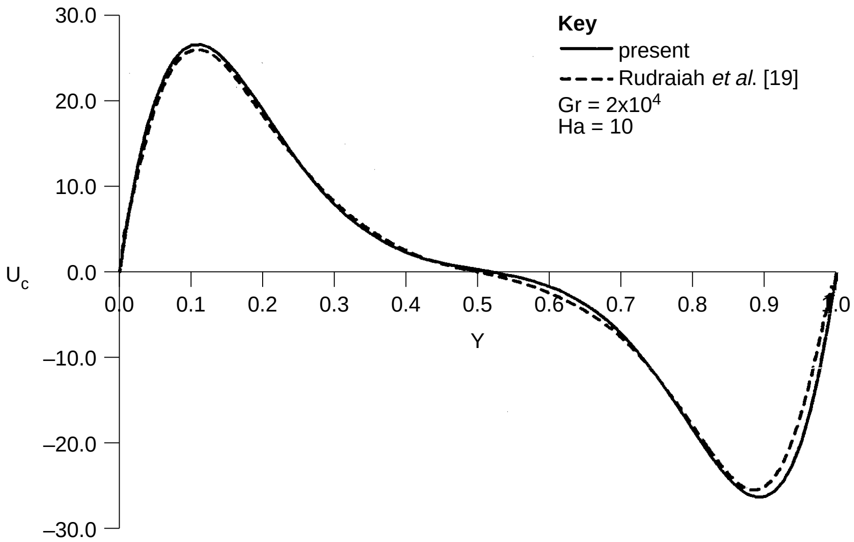

Figure 3.
Comparison of the horizontal velocity profile between the present prediction and other numerical results

one can conclude that the main contribution of the magnetic effect is to suppress the overall heat transfer between the hot and cold walls.

At high Grashof number ($Gr = 1 \times 10^6$), a similar study is conducted to examine the effect of the magnetic field (Ha) and inclination angle (α) on the flow patterns and isotherms inside the tilted enclosure, and the results are given in Figures 8 and 9. As predicted by Barakos *et al.*[11], the core vortex breaks up in two vortices with the increase of Grashof number, see Figures 6 and 9. The two vortices move towards the vertical walls giving space for a third vortex to develop. This third vortex is very weak in comparison with the other two vortices (Figure 8), as discussed in detail by other investigators[29,30]. The flow rotation in this third vortex is clockwise owing to a very small positive temperature gradient at the center of the cavity. The velocities in the core of the cavity are very small compared with those at the boundaries where the fluid is moving fast, forming vortices at the lower right and top left corner of the cavity. These vortices are narrow enough to impose stratification of the flow at the center part of the cavity. The shape of the isotherms shows how the dominant heat transfer mechanism changes as Grashof number increases. For low Grashof numbers, Figure 6, heat transfer between the hot and cold walls is carried out by conduction and convection. As the Grashof number increases to 1×10^6, the heat transfer mechanism changes to a relatively pure convection, Figure 9. The flow patterns as illustrated in Figure 8 shows that there is a strong upward flow near the heated side wall and downward flow at the cold wall. For high Grashof number and weak magnetic field strength (Ha = 15), a vertical temperature stratification (i.e. almost zero temperature gradients in the horizontal direction) is well established at the core, Figure 8. This indicates very thin vertical thermal boundary layers are formed along the side walls and a

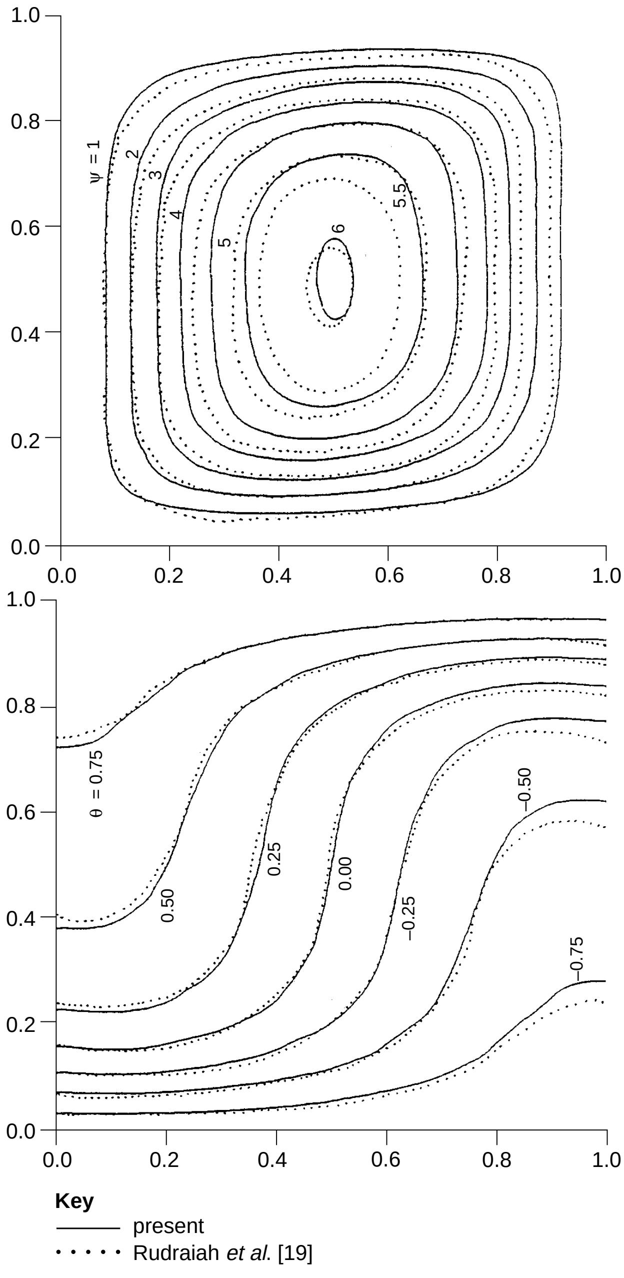

Figure 4.
Comparison of the flow patterns and isotherms between the present prediction and Rudraiah *et al.*[19] at Gr = 2×10^4 and Ha = 10

dominant convection heat transfer mechanism in the core. At the same time, Figure 8 indicates that as Hartmann number increases, the temperature stratification in the core diminishes and the thermal boundary layers at the two side walls disappear. This process is accompanied by the movement of the two side vorticies towards the horizontal center line of the cavity until they combine together to form one central vortex at high Hartmann number (Ha = 50). Further, when Hartmann number increases to 100, the axis of this central vortex is rotated counterclock wise. This is due to the retarding effect of the Lorentz force.

Typical temperature and velocity profiles in a vertical cavity ($\alpha = 0$) for various values of Hartmann and at low Grashof numbers at mid-sections of the cavity are given in Figure 10. The application of a transverse magnetic field results in a force opposite to the flow direction which tends to drag the flow (i.e. decreasing the horizontal velocity at the centerline). Also, the conduction heat transfer mechanism becomes dominant as Hartmann number is increased. This is clearly noticed in the temperature profiles at the center of the cavity given in Figure 10. Hence, the effect of this force becomes greater as the strength of the magnetic field increases. It is clear that the decrease in temperature and velocity is due to the increase in Hartmann number. At high Grashof number ($Gr = 1 \times 10^6$) the influence of the magnetic field is weaker. The temperature profiles at very high Hartmann number (Ha = 100), indicates that the heat transfer process is not totally carried out by pure conduction (compared with low Grashof number) but still controlled by both conduction and convection mechanisms.

Finally, the effects of the inclination angle (α) and the Hartmann number on the average Nusselt number at high and moderate Grashof numbers is shown in Figure 11. As discussed earlier, for high Hartmann number the only resistance to the flow is due to the magnetic drag and the resulting convective heat transfer is diminished. Thus, as $Ha \rightarrow \infty$, the Nusselt number approaches unity, indicating a pure conduction regime. Furthermore, it is observed from Figure 11 that as the value of Ha is increased, the heat transfer is reduced, for a given inclination angle, because the viscous effects along with the magnetic drag reduce the fluid circulation. In Figure 11a, the rate of variation of the Nusselt number with tilting angle is almost constant ($0 < |\alpha| < 80$) and depends only on the Hartmann number. On the other hand, for high Grashof number, Figure 11b, the value of Nusselt number depends strongly upon the inclination angle for relatively small values of Hartmann number. Moreover, it is noticed that there is

	$\overline{Nu}$
Present results	2.249
De Vahl Devis[4]	2.243
Barakos *et al.*[11]	2.245
Markatos and Pericleous[30]	2.201
Fusegi *et al.*[31]	2.302
Newell and Schmidt[32]	1.96[a]

Note:
[a]Obtained from the correlation formula given by Newell and Schmidt[32]

Table II. Comparison of the average Nusselt number between the present prediction and other numerical results ($Ra = 1 \times 10^4$, Ha = 0 and Pr = 0.71)

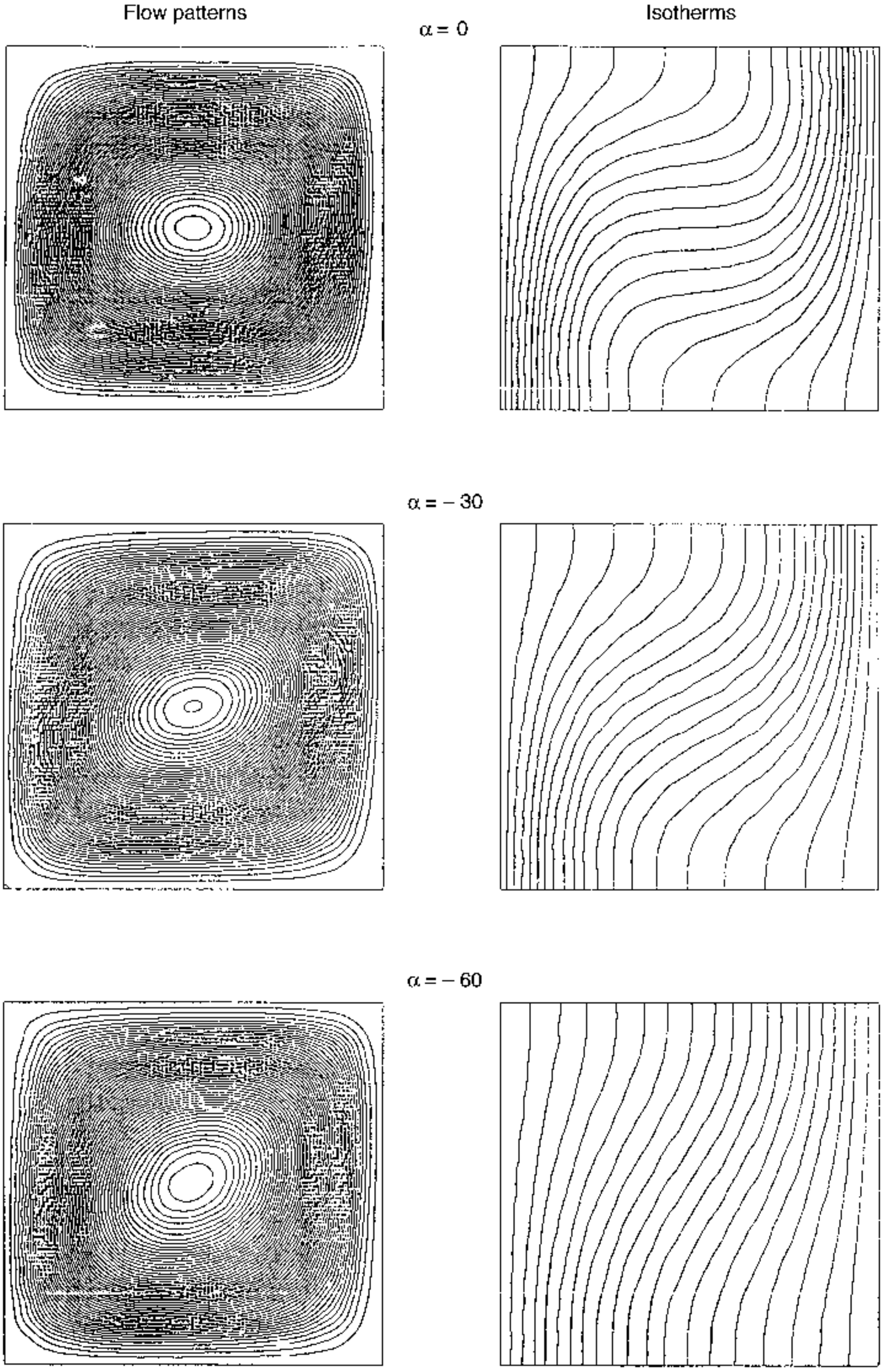

Figure 5.
Flow patterns and isotherms for different inclination angles at $Gr = 1 \times 10^4$ and $Ha = 0$

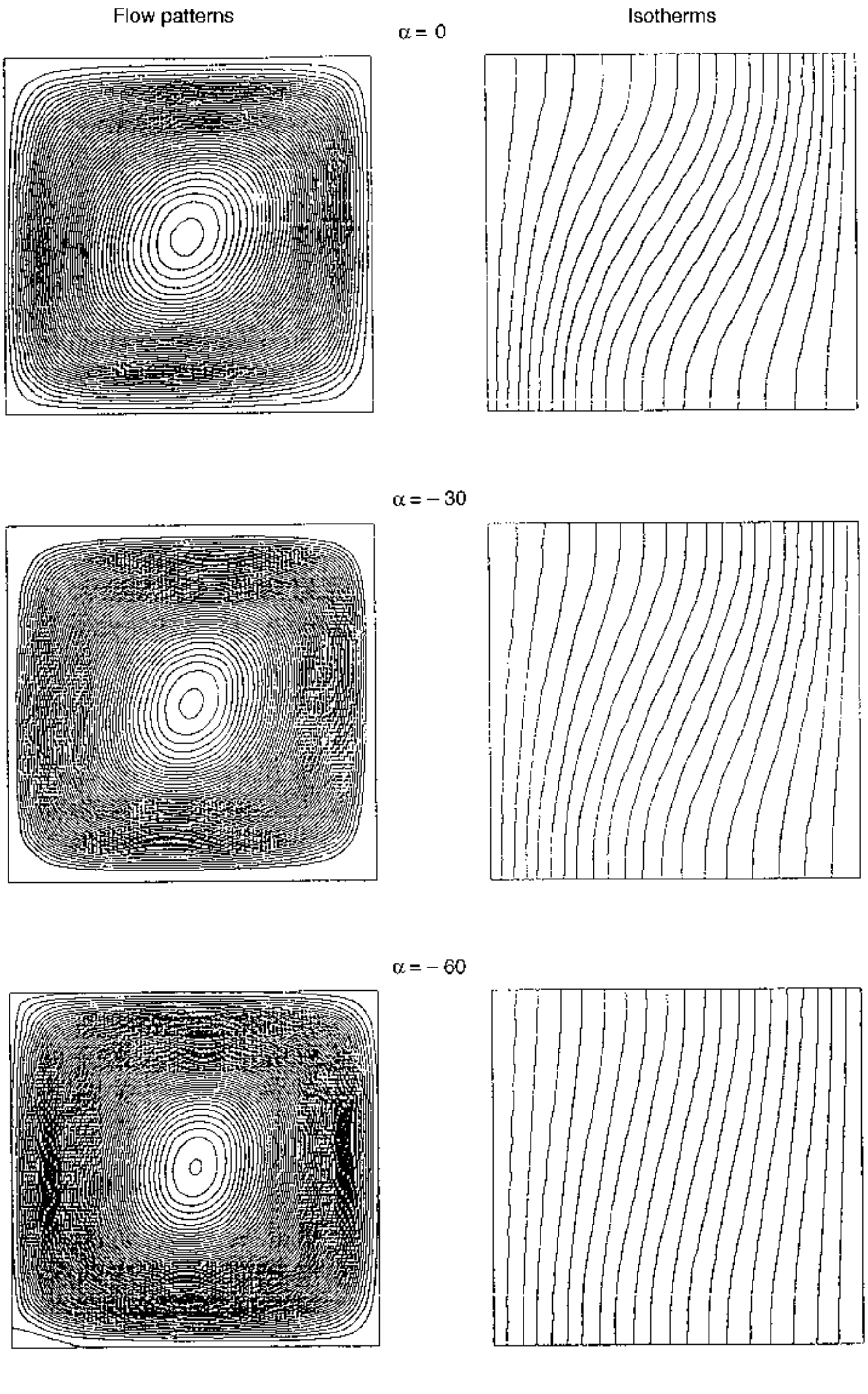

Figure 6.
Flow patterns and isotherms for different inclination angles at $Gr = 1 \times 10^4$ and $Ha = 25$

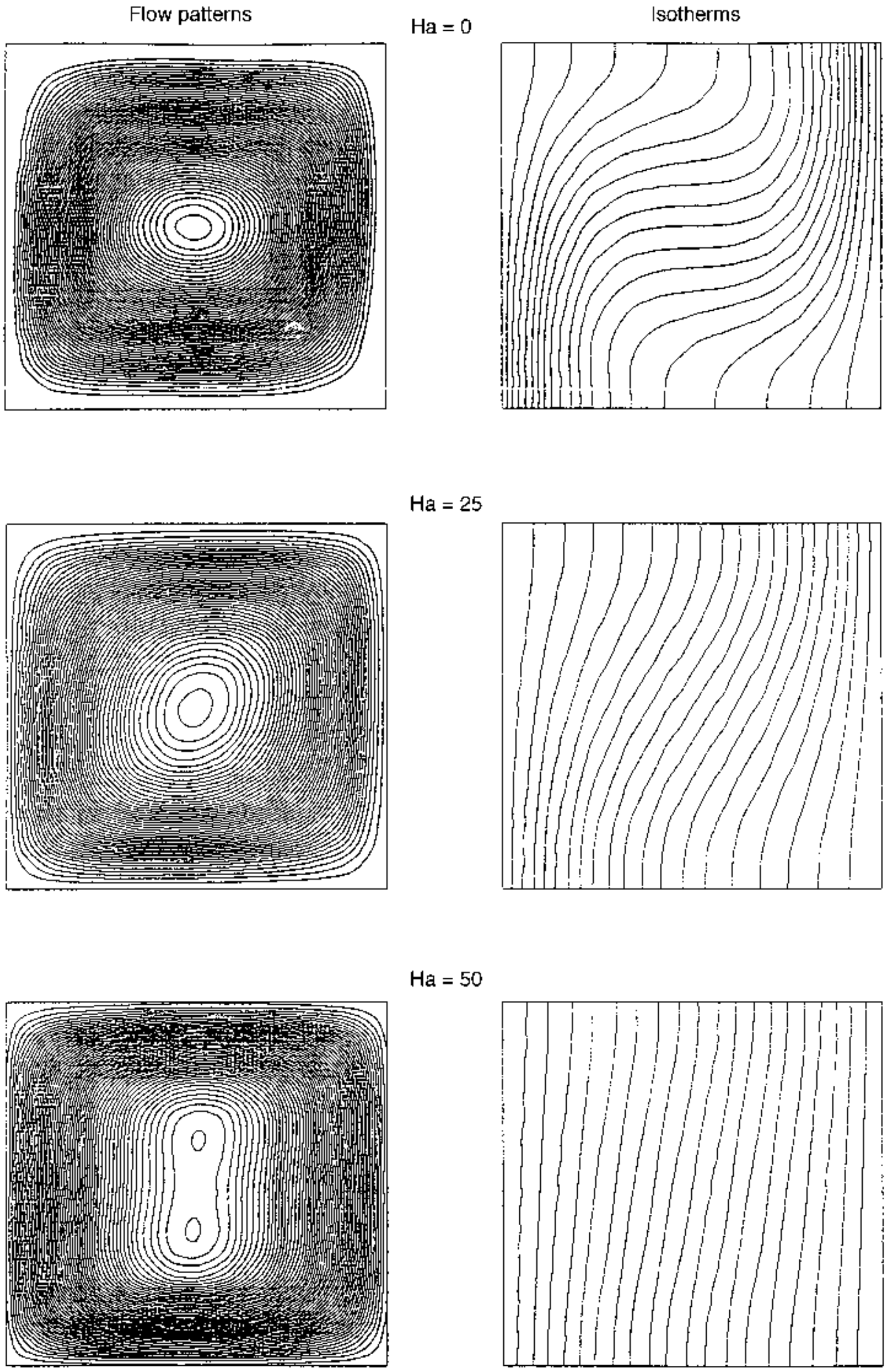

Figure 7.
Flow patterns and isotherms for different Hartmann numbers at $Gr = 1 \times 10^4$ and $\alpha = 0$

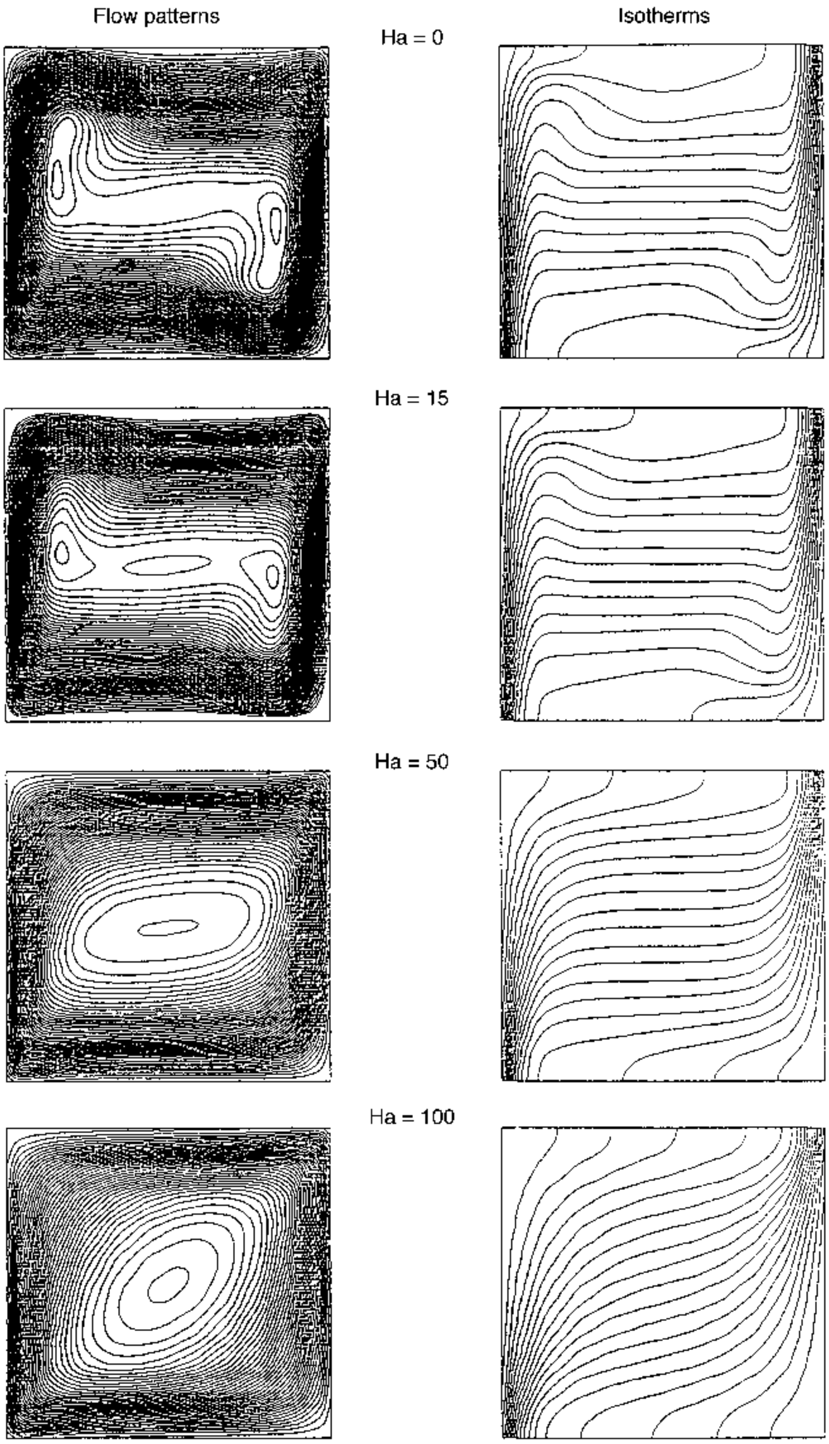

Figure 8.
Flow patterns and isotherms for different Harmann numbers at $Gr = 1 \times 10^6$ and $\alpha = 0$

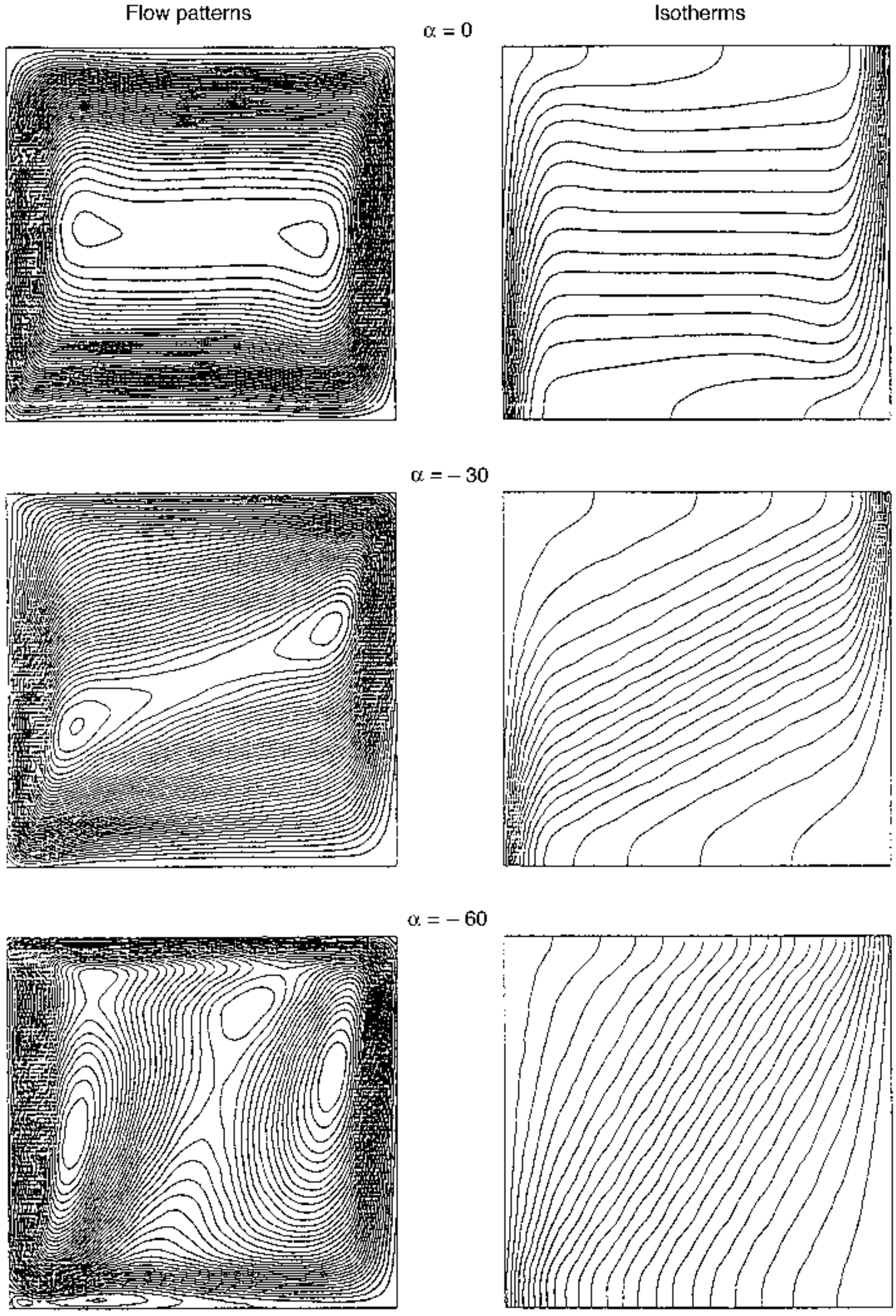

Figure 9.
Flow patterns and isotherms for different inclination angles at $Gr = 1 \times 10^6$ and $Ha = 25$

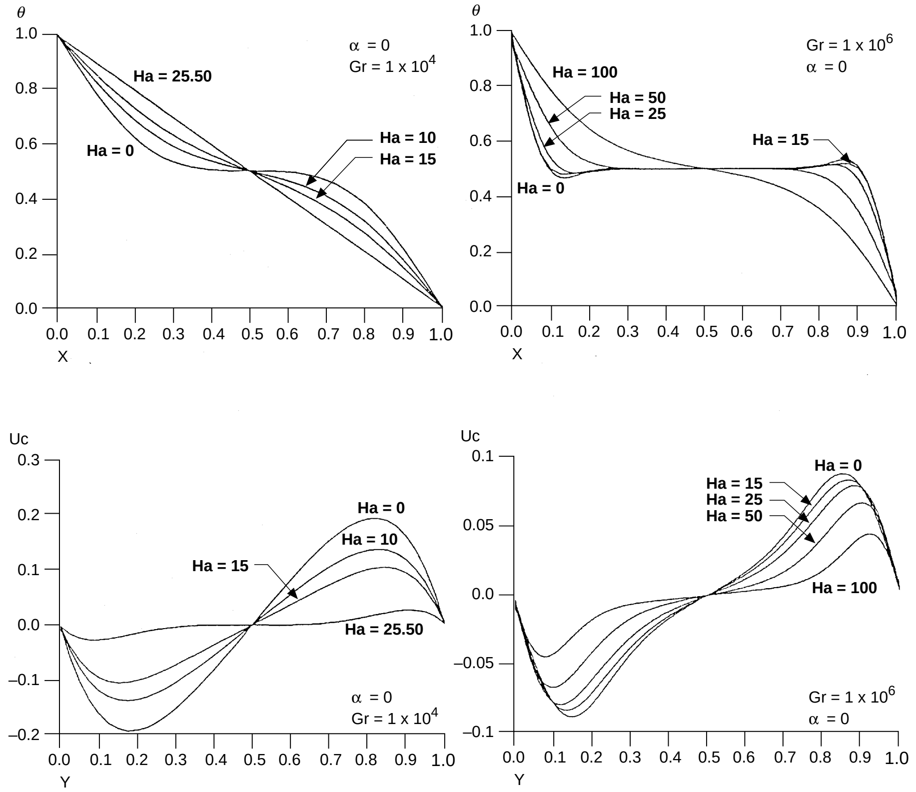

Figure 10.
Temperature and velocity profiles at mid-sections of the cavity for different values of Ha

no variation of average Nusselt number with respect to tilting angle for high Hartmann number.

Conclusions

The present numerical study shows interesting features concerning the effect of transverse magnetic field at both moderate and high Grashof numbers on the natural convection flows in tilted enclosures. The prediction is in good agreement with available published work in the literature. Detailed numerical experiments for the flow field and heat transfer are given. Inspecting the numerical simulations reveals the following conclusions:

(1) The heat transfer mechanisms and the flow characteristics inside the tilted enclosures depend strongly upon both the strength of the magnetic field and the inclination angle. Significant suppression of the convective current can be obtained by applying strong magnetic field.

(2) The effect of the magnetic field considerably decreases the Nusselt number at low Grashof number than at higher values.

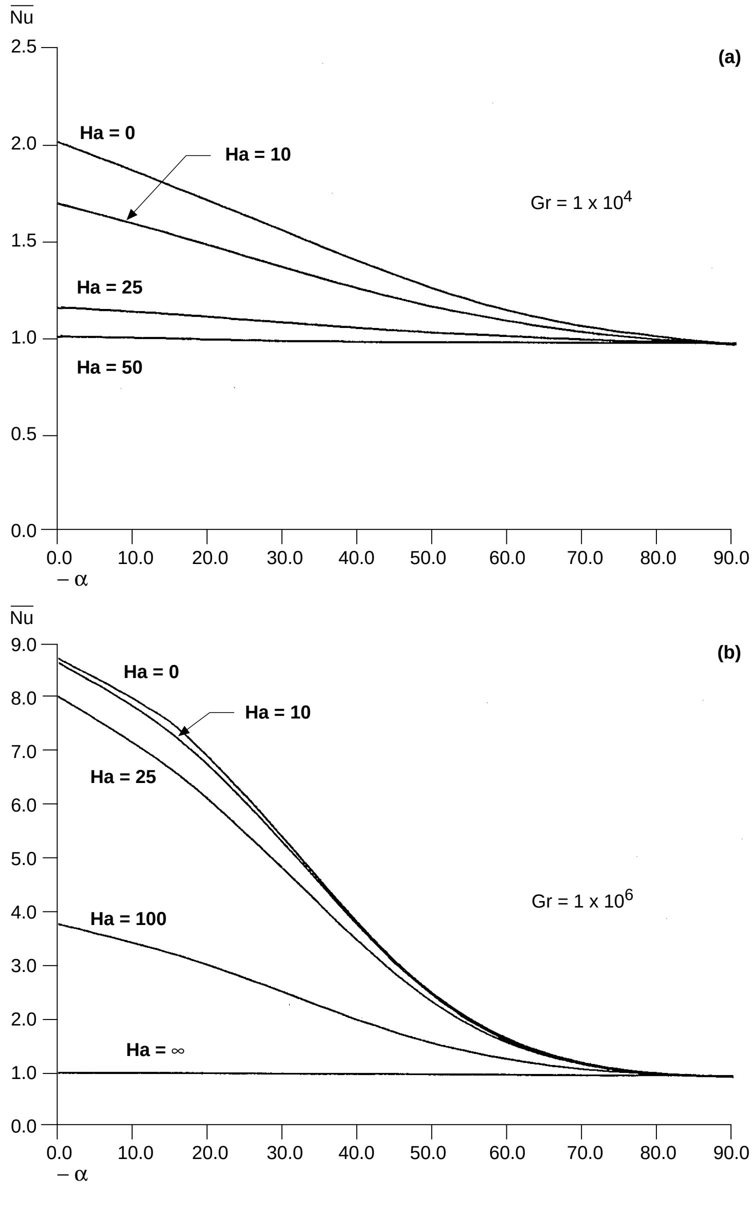

Figure 11.
Effect of inclination angle α and Hartmann number Ha on the average Nusselt number $\overline{Nu}$

(3) The magnetic field has negligible effect on the heat transfer mechanism for small inclination angles. This is true since pure conduction becomes the dominant when the inclination angle approaches –90°.

It should be pointed out that the general analysis described in this work should represent a useful starting point to treat more complex problem, such as turbulent and time-dependent flows. It is expected that the imposition of external magnetic field may play a very important role in suppressing turbulence or time-unsteadiness.

References

1. Ostrach, S., “Natural convection in enclosures”, in Hartnett, J.P. and Irvine, T.F. (Eds), *Advances in Heat Transfer*, Vol. 8, Academic Press, New York, NY, 1972, pp. 161-227.
2. Catton, I., “Natural convection in enclosures”, *Proceedings of the Sixth International Heat Transfer Conference*, Toronto, Vol. 6, August 1978, pp. 13-31.
3. Bejan, A. and Tien, C.L., “Laminar natural convection heat transfer in a horizontal cavity with different end temperatures”, *ASME Journal of Heat Transfer*, Vol. 100, November 1978, pp. 641-7.
4. De Vahl Davis, G., “Natural convection of air in a square cavity: a bench mark numerical solution”, *Int. J. for Numer. Methods in Fluids*, Vol. 3, 1983, pp. 249-64.
5. Krane, R.J. and Jessee, J., “Some detailed field measurements for a natural convection flow in a vertical square enclosure”, *Proc. 1st. ASME-JSME Thermal Engineering Joint Conf.*, Vol. 1, 1983, pp. 323-9.
6. Gou, K.L. and Wu, S.T., “Numerical study of flow and temperature stratifications in a liquid thermal storage tank”, *Journal of Solar Energy Engineering*, Vol. 107, February 1985, pp. 15-20.
7. Hall, J.D., Bejan, A. and Chaddock, J.B., “Transient natural convection in a rectangular enclosure with one heated side wall”, *Int. J. Heat and Fluid Flow*, Vol. 9 No. 4, December 1988, pp. 396-404.
8. Patterson, J.C. and Armfield, S.W., “Transient features of natural convection in a cavity”, *J. Fluid Mechanics*, Vol. 219, 1990, pp. 469-97.
9. Kuyper, R.A., Van Der Meer, T.H., Hoogendoorn, C.J. and Henkes, R.A.W.M, “Numerical study of laminar and turbulent natural convection in an inclined square cavity”, *Int. J. Heat Mass Transfer*, Vol. 36 No. 11, 1993, pp. 2899-911.
10. Ravi, M.R., Henkes, R.A.W.M. and Hoogendoorn, C.J., “On the high-Rayleigh-number structure of steady laminar natural-convection flow in a square enclosure”, *J. Fluid Mechanics*, Vol. 262, 1994, pp. 325-51.
11. Barakos, G., Mitsoulis, E. and Assimacopoulos, D., “Natural convection flow in a square cavity revisited: laminar and turbulent models with wall functions”, *Int. J. Numer. Methods Fluids*, Vol. 18, 1994, pp. 695-719.
12. Janssen, R.J.A. and Henkes, R.A.W.M., “Influence of Prandtl number on instability mechanisms and transition in a differentially heated square cavity”, *J. Fluid Mechanics*, Vol. 290, 1995, pp. 319-44.
13. Ozoe, H. and Maruo, M., “Magnetic and gravitational natural convection of melted silicon-two dimensional numerical computations for the rate of heat transfer”, *J.S.M.E.*, Vol. 30, 1987, pp. 774-84.
14. Ozoe, H. and Okada, K., “The effect of the direction of the external magnetic field on the three-dimensional natural convection in a cubical enclosure”, *Int. J. Heat Mass Transfer*, Vol. 32 No. 10, 1989, pp. 1939-54.
15. Vasseur, P., Hasnaoui, M., Bilgen, E. and Robillard, L., “Natural convection in an inclined fluid layer with a transverse magnetic field: analogy with a porous medium”, *ASME Journal of Heat Transfer*, February 1995, Vol. 117, pp. 121-9.
16. Cormack, D.G., Leal, L.G. and Imberger, J., “Natural convection in a shallow cavity with differentially heated end qalls: Part 1, asymptotic theory”, *J. Fluid Mechanics*, Vol. 65, 1974, pp. 209-30.

17. Alchaar, S., Vasseur, P. and Bilgen, E., "Natural convection heat transfer in a rectangular enclosure with a transverse magnetic field", *ASME Journal Heat Transfer*, Vol. 117, August 1995, pp. 668-73.
18. Garandet, J.P., Alboussiere, T. and Moreau, R., "Bouyancy drive convection in a rectangular enclosure with a transverse magnetic field", *Int. J. Heat Mass Transfer*, Vol. 35 No. 4, 1992, pp. 741-8.
19. Rudraiah, N., Barron, R.M., Venkatachalappa, M. and Subbaraya, C.K., "Effect of a magnetic field on free convection in a rectangular enclosure", *Int. J. Engng Sci.*, Vol. 33 No. 8, 1995, pp. 1075-84.
20. Oreper, G. M. and Szekely, J., "The effect of an externally imposed magnetic field on bouyancy driven flow in a rectangular cavity", *Journal of Crystal Growth*, Vol. 64, 1983, pp. 505-15.
21. Alchaar, S., Vasseur, P. and Bilgen, E., "The effect of a magnetic field on natural convection in a shallow cavity heated from below", *Chem. Eng. Comm.*, Vol. 134, 1995, pp. 195-209.
22. Kakac, S.S., Shah, R.K. and Aung, W., *Handbook of Single-Phase Convection Heat Transfer*, John Wiley & Sons, 1987.
23. Kakac, S., Aung, W. and Viskanta, R., *Natural Convection – Fundamentals and Applications*, Hemisphere, Washington, DC, 1985.
24. Sathe, S.B., Lin, W.Q. and Tong, T.W., "Natural convection in enclosures containing an insulation with a permeable fluid-porous interface", *Int. J. Heat and Fluid Flow*, Vol. 9 No. 4, December 1988.
25. El-Refaee, M.M., El-Sayed, M.M., Al-Najem, N.M. and Megahid, I.E., "Steady-state solutions of buoyancy-assisted internal flows using a fast false implicit transient scheme (FITS)", *Int. J. of Numer. Methods for Heat and Fluid Flow*, Vol. 6 No. 6, 1996, pp. 3-23.
26. Versteeg, H.K. and Malalasekera, W., *An Introduction to Computational Fluid Dynamics – The Finite Volume Approach*, Longman Scientific & Technical, 1995.
27. Patankar, S.V., *Numerical Heat Transfer and Fluid Flow*, Hemisphere, Washington, DC, 1980.
28. Khanafer, K.M., "Numerical study of laminar natural convection in tilted enclosure with transverse magnetic field", Master Thesis, Kuwait University, 1996.
29. De Vahl Davis, G., "Laminar natural convection in an enclosed rectangular cavity", *Int. J. Heat Mass Transfer*, Vol. 11, 1968, pp. 1675-93.
30. Markatos, N.C. and Pericleous, K.A., "Laminar and turbulent natural convection in an enclosed cavity", *Int. J. Heat Mass Transfer*, Vol. 27, 1984, pp. 772-5.
31. Fusegi, T., Hyun, J.M., Kuwahara, K. and Farouk, B., "A numerical study of three-dimensional natural convection in a differentially heated cubical enclosure", *Int. J. Heat Transfer*, Vol. 34, 1991, pp. 1543-57.
32. Newell, M.E. and Schmidt, F.W., "Natural convection heat transfer in square enclosures", *J. Heat Transfer*, Vol. 92, 1970.